The role of the divalent cation in the structure of the I domain from the CD11a/CD18 integrin

Aidong Qu and Daniel J Leahy*

Background: The integrin family of cell-surface receptors mediates a wide variety of cell–cell and cell–extracellular matrix interactions. Integrin–ligand interactions are invariably dependent on the presence of divalent cations, and a subset of integrins contain a ~200 amino acid inserted (I) domain that is important for ligand binding activity and contains a single divalent cation binding site. Many integrins are believed to respond to stimuli by undergoing a conformational change that increases their affinity for ligand, and there is a clear difference between two crystal structures of the CD11b I domain with different divalent cations (magnesium and manganese) bound. In addition to the different bound cation, a 'ligand mimetic' crystal lattice interaction in the CD11b I domain structure with bound magnesium has led to the interpretation that the different CD11b I domain structures represent different affinity states of I domains. The influence of the bound cation on I domain structure and function remains incompletely understood, however. The crystal structure of the CD11a I domain bound to manganese is known. We therefore set out to determine whether this structure changes when the metal ion is altered or removed.

Results: We report here the crystal structures of the CD11a I domain determined in the absence of bound metal ion and with bound magnesium ion. No major structural rearrangements are observed in the metal-binding site of the CD11a I domain in the absence or presence of bound manganese ion. The structures of the CD11a I domain with magnesium or manganese bound are extremely similar.

Conclusions: The conformation of the CD11a I domain is not altered by changes in metal ion binding. The cation-dependence of ligand binding thus indicates that the metal ion is either involved in direct interaction with ligand or required to promote a favorable quaternary arrangement of the integrin.

Address: Department of Biophysics and Biophysical Chemistry, Johns Hopkins University School of Medicine, 725 N. Wolfe Street, Baltimore, MD 21205, USA.

*Corresponding author.
E-mail: leahy@cthulu.med.jhu.edu

Key words: anomalous diffraction, MAD, magnesium, manganese, selenomethionine, X-ray

Received: 9 May 1996
Revisions requested: 4 June 1996
Revisions received: 19 June 1996
Accepted: 25 June 1996

Structure 15 August 1996, 4:931–942

Introduction

Members of the integrin family of cell-surface receptors are typically involved in some aspect of cell adhesion through interactions with components of the extracellular matrix or other cell-surface receptors [1]. Integrins are non-covalently associated heterodimers consisting of a 120–180 kDa α chain and a 90–120 kDa β chain. Both α and β chains are single-pass transmembrane proteins with large extracellular components and variable but generally small cytoplasmic regions. Over 20 different integrins have been identified with many integrins sharing common subunits. The CD11a/CD18 (LFA-1, $\alpha_L\beta_2$) integrin is expressed on all leukocytes and mediates adhesion to a variety of cell types that express one or more of the CD11a/CD18 ligands, the intercellular adhesion molecules (ICAMs), ICAM-1, ICAM-2, or ICAM-3. The processes mediated by CD11a/CD18 interactions include adhesion to the endothelium and extravasation at sites of inflammation and adherence of activated T cells to target cells [2].

Integrins have been shown to transmit signals in both directions across the cell membrane [1]. Interactions of an integrin with ligand have been shown to alter the behavior or properties of the integrin-bearing cell, and the affinity of many integrins for ligand is increased following appropriate cellular stimuli. This increase in affinity is believed to be accompanied by conformational changes in the integrin [1,3]. Interactions of integrins with ligands are dependent on the presence of divalent cations, with Mg^{2+} being the likely physiological cation in most circumstances. Several integrins have a higher affinity for Mn^{2+}, however, and Mn^{2+} is capable of inducing the high-affinity state of these integrins in the absence of other stimuli [4–6].

A subset of integrin α chains, including CD11a, contain an inserted or 'I' domain of ~200 amino acids. I domains belong to a family of homologous domains of which von Willebrand factor 'A' domains are the prototype [7,8]. In each of these integrins the I domain has been shown to provide a large component of ligand-binding activity [6,9–14]. The crystal structures of the CD11b I domain with bound magnesium [15] and the CD11a and CD11b I domains with bound manganese [16,17] have recently been determined and reveal these domains to possess a

flavodoxin-like dinucleotide-binding fold [18,19]. Instead of a dinucleotide cofactor, however, the I domains bind a divalent cation through a conserved amino acid sequence motif Asp-X-Ser-X-Ser (DXSXS). The presence of this sequence motif in integrin β chains together with a conserved pattern of hydrophobicity between I domains and this region in integrin β chains has led to speculation that integrin β chains may also contain an I domain-like structure [15]. Mutations of the divalent cation binding motif in both I domains and integrin β chains impair ligand binding [6,20–22].

The mechanisms by which integrins increase their affinity for ligand and the role that divalent cations play in both activation and ligand binding remain incompletely understood. Two nonexclusive mechanisms have been proposed to explain the metal dependence of integrin–ligand interactions. The first mechanism proposes that the metal may be required to stabilize an active tertiary or quaternary conformation of the integrin; the second that the integrin-bound metal ion may participate directly in interactions with ligand, possibly through interactions between the metal ion and an acidic residue in the ligand. The frequent occurrence of acidic amino acids in the ligand- binding sites recognized by integrins [1] and a direct interaction between a glutamic acid side chain from an adjacent molecule in the crystal lattice and a bound magnesium ion in the CD11b I domain crystal structure [15] have been cited as indications that the metal ion participates directly in ligand binding. A series of mutations in the CD11a I domain that abolish ligand binding also map in the vicinity of the metal-binding surface [22]. Other studies, however, have suggested that cation and ligand binding are separable properties of integrins [21,23], and a region of the CD11a I domain that is critical for ICAM-3 binding maps to a region diametrically opposite the metal-binding surface [24].

A molecular understanding of the differing effects of specific cations on ligand binding by integrins also remains elusive. The nature of the metal coordination differs between the structure of the CD11b I domain with bound magnesium, and the structures of the CD11a and CD11b I domains with bound manganese, despite conservation of the amino acids that interact with the metal ion and octahedral coordination geometry. Differences in the metal-binding site structure of the CD11b I domain with bound magnesium or bound manganese appear correlated with additional structural changes, particularly differences in an α helix, α7. These differences have been proposed to reflect high- and low-affinity states of the I domain [17]. The amino acid sequence similarity (36% identity between CD11a and CD11b with 33% identity in the I domains [7]) and the consequent structural similarity, the conserved metal-binding motif, a common β subunit, and similar activation behavior suggest that the structural features of activation will be similar for the CD11a/CD18 and CD11b/CD18 integrins.

To evaluate the effects of metal binding on I domain structure we have determined and report here the crystal structure of the CD11a I domain in the absence of bound metal ion. To evaluate the influence of the specific metal ion bound versus the effects of a 'ligand mimetic' crystal lattice interaction on I domain structure, we have also determined and report here the crystal structure of the CD11a I domain with bound magnesium ion. These structures are compared with the previously determined structure of the CD11a I domain with bound manganese ion.

Results

Determination of the metal-free structure of the CD11a I domain

The crystal structure of a metal-free form of the CD11a I domain (CD11a-I(EDTA)) was solved by the multi-wavelength anomalous diffraction (MAD) method. MAD-phased electron-density maps allowed confident placement of all residues in CD11a-I(EDTA) except for the four N-terminal residues (Cys125–Gly128) and 15 C-terminal residues (Lys297–Gly311). Sufficient electron density was present for residues 297 to 308 to determine that these residues form a helical structure and to trace the general course of this helix. Inclusion of these residues in the atomic model resulted in a 0.4% decrease in the free R value [25]. However, atomic positions for these residues are poorly defined, with an average B factor of 63 $Å^2$ for residues 297–308. Inspection of both experimentally-phased electron-density maps and difference maps calculated during refinement confirmed the absence of a divalent cation in the conserved metal-binding site of CD11-I(EDTA) (see Fig. 1a). Data collection results, refinement statistics, and stereochemical parameters for the CD11a-I(EDTA) structure are shown in Tables 1–3.

Determination of the manganese- and magnesium-bound structures of the CD11a I domain

Crystals of the CD11a I domain refolded in the presence of Mg^{2+}, CD11a-I(Mg), remained relatively small and diffraction data beyond 2.8–3.0 Å Bragg spacings could not be accurately measured. Virtually isomorphous crystals of the CD11a I domain with bound manganese, CD11a-I(Mn), were obtained, however, that diffracted to at least 2.0 Å Bragg spacings. The structure of CD11a-I(Mn) in this new space group $P2_12_12$ was solved by molecular replacement using the structure of this domain previously determined in the space group C2 [16] as a search model. The asymmetric unit of the $P2_12_12$ crystal form contained two molecules of the CD11a I domain arranged identically to the two molecules in the asymmetric unit of the C2 crystal form, and the molecular replacement solution refined easily to low R factor. The common arrangement of the

Figure 1

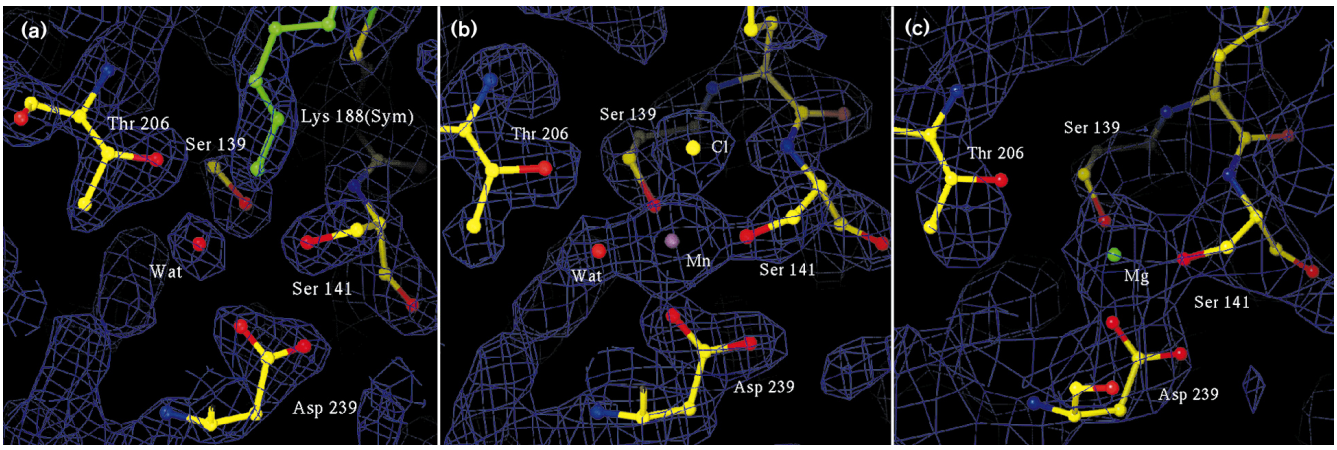

Simulated annealing omit maps [26] of the CD11a metal-binding site in the presence and absence of divalent cation contoured at 1.2σ: **(a)** CD11a-I(EDTA) calculated at 2.0 Å, **(b)** CD11a-I(Mn) calculated at 2.0 Å, and **(c)** CD11a-I(Mg) calculated at 3.0 Å. The maps are displayed with the final model positions of residues Asp137–Ser141, Thr206, Asp239, and any water molecules or metal ions in the metal-binding site. Water molecules are shown as red spheres, manganese and magnesium ions are in purple and green, respectively. In (b) an additional water molecule bound to the manganese ion has been clipped from view for clarity. In all structures atoms within an 8 Å sphere around the metal ion were omitted from refinement and map calculations. (Figure made with the program O [40].)

independent molecules in the asymmetric units of both the C2 and $P2_12_12$ crystal forms involves an interaction of the C termini of the adjacent molecules that appears to influence the disposition of the α7 helix relative to the rest of the molecule. Gel filtration chromatography reveals that, in the presence of Mn^{2+}, the CD11a I domain exists in an equilibrium between monomer and dimer in solution (data not shown). The involvement of the artificially-truncated C terminus of the I domain in the dimer interaction indicates that this interaction is unlikely to be physiologically relevant. Refinement statistics and stereochemical parameters for the $P2_12_12$ CD11a-I(Mn) structure are shown in Table 4.

Simulated annealing omit maps [26] confirmed that the manganese coordination is identical in the C2 and $P2_12_12$ crystal forms. As shown in Figure 1b, the manganese ion is directly coordinated by Ser139, Ser141, and Asp239 while Thr206 makes a hydrogen bond to one of two manganese-bound waters. The coordination geometry is octahedral, and an apparent chloride ion is the sixth metal ligand. A chloride ion is presumed for several reasons; the characteristic interatomic distance (~2.5 Å); the observed intensity of the scatterer at this site; the resulting neutrality of the manganese coordination sphere if this site is occupied by a monovalent anion; and chloride is the only monovalent anion added to the crystallization mixture. The root mean square (rms) deviations in Cα positions between the independent CD11a I domains in the C2 and $P2_12_12$ crystal forms are 0.23–0.26 Å; these values are comparable to the differences found between the independent molecules within the asymmetric unit of either crystal form.

The virtual isomorphism of the $P2_12_12$ crystal forms of the CD11a I domain refolded in either Mn^{2+} or Mg^{2+} allowed the determination of the Mg^{2+} structure by rigid-body

Table 1

Data collection statistics for CD11a-I(EDTA).

Data collection statistics (30.0 to 2.2 Å)

Wavelength (Å)	Number of reflections (N)	Redundancy	Completeness* (%)	Signal (<I/σI>)	R_{sym}* (%)
0.9879	8476	9.7	97.0	19.2	11.1
0.9793	8526	10.2	97.6	19.1	11.7
0.9791	8513	9.8	97.4	19.0	11.4
0.9686	8544	10.0	98.0	18.8	11.9

*R_{sym} and completeness values were calculated considering Bijvoets equivalent. $R_{sym}=100\times\Sigma_h\Sigma_i\,|I_i(h)-\langle I(h)\rangle|\,/\Sigma_h\Sigma_i I_i(h)$.

Table 2

MAD structure factor ratios and anomalous scattering factors for CD11a-I(EDTA).

Wavelength (Å)	Wavelength (Å)				Anomalous scattering factors	
	0.9879	0.9793	0.9792	0.9686	f′ (e)	f″ (e)
0.9879	0.047	0.073	0.066	0.070	-4.28	0.51
0.9793		0.065	0.053	0.078	-9.73	3.87
0.9791			0.076	0.071	-7.92	5.36
0.9686				0.063	-3.61	4.00

MAD structure factor ratios calculated using (rms[Δ|F|])/(rms[|F|]) where ΔF is the Bijvoet difference at one wavelength (diagonal elements) or the dispersive difference between two wavelengths (off diagonal elements). Centric data were merged to a single value and are thus not shown. The Bijvoet difference at the 0.9870 Å wavelength may be taken instead as an upper limit of the noise of the anomalous signals. Also shown are the anomalous components of the Se scattering factors as a function of wavelength as determined by MADLSQ [35].

refinement of the Mn^{2+}-containing structure. To avoid potential model bias from the metal-binding region of the Mn^{2+} structure, a simulated annealing refinement of the Mn^{2+} structure was carried out prior to the rigid-body refinement. In this simulated-annealing, refinement atoms within an 8 Å sphere of the manganese ion in one of the molecules in the asymmetric unit were omitted from the refinement calculations. An independent simulated annealing refinement was carried out in which a similar sphere around the manganese ion bound to the other I domain in the crystallographic asymmetric unit was omitted from refinement calculations. Rigid-body refinement of these models with the CD11a-I(Mg) diffraction data resulted in an R factor of 0.279 with an R free of 0.269 for all data 10–3.0 Å. Inspection of $(2F_o–F_c)e^{i\phi calc}$ difference maps led to the repositioning of nine amino acid side chains in the CD11a-I(Mg) model which resulted in an R factor of 0.279 and an R free of 0.264 without refinement. All attempts to further refine the rigid-body solutions, while significantly reducing the R factor, resulted in increases in R free, and no further refinement was thus performed. Figure 1c shows a simulated annealing omit map from which an 8 Å sphere around the magnesium ion has been omitted from the map calculation [26]. While the lower resolution of the Mg^{2+} structure does not permit evaluation of the precise detail of the solvent molecules involved in the magnesium coordination, it is clear that Ser139, Ser141, and Asp239 directly coordinate the magnesium ion while Thr206 does not. A similar result was obtained when the region surrounding the magnesium ion in the other molecule in the asymmetric unit was omitted from the map calculation.

Table 3

Final refinement and stereochemical statistics for CD11a-I(EDTA).

R value	
(F>2σ, 6.0–2.0 Å)	0.184
(all F, 6.0–2.0 Å)	0.198
R_{free}	
(F>2σ, 6.0–2.0 Å)	0.243
(all F, 6.0–2.0 Å)	0.252
Average B (Å^2)	
for protein	21.92
for solvent	29.24
Rms deviations	
bonds (Å)	0.009
angles (°)	1.90
B values (Å^2)	
bonds/angles of main chains	0.98/1.10
bonds/angles of side chains	1.74/1.82

A subset of the data (5%) was excluded from refinement and used for the free R value calculation [25]. All data for which |F|>2σ were used in the refinement. R value=$\Sigma||F_o|–|F_c||/\Sigma|F_o|$.

Comparison of CD11a-I(EDTA) and CD11a-I(Mn) structures

With the exception of a large shift in the position of the C terminus of the α7 helix, the structure of CD11a-I(EDTA) is very similar to the structure of CD11a-I(Mn) [16]. Owing to the similarity of the CD11a-I(Mn) structures determined in different crystal forms (packing of the common dimer in the asymmetric unit is very similar in the C2 and $P2_12_12$ crystal forms), one of the molecules in the asymmetric unit of the C2 crystal form was used as a representative structure for comparisons. All I domain structures, including those reported here, consist of a flavodoxin-like dinucleotide-binding fold [18,19] with a core parallel β sheet surrounded by α helices. Figure 2a shows a ribbon diagram of the CD11a-I(EDTA) structure, and Figure 2b shows a stereo view of a superposition of the Cα backbones of CD11a-I(EDTA) and CD11a-I(Mn). Figure 3 shows the distance between Cα atoms at each amino acid position following superposition of the CD11a-I(EDTA) and CD11a-I(Mn) structures. Distances between Cα atoms of greater than 1.0 Å are observed in four places in the CD11a-I structures: three loop regions (β1–α1, α4–β3 and β4–α6) and the C terminus including a portion of the α7 helix. With the exception of the α4–β3 connection, each of

Table 4

Data collection and refinement statistics.

	CD11a-I(Mn)*	CD11a-I(Mg)†
Data collection statistics		
Wavelength (Å)	1.54	1.54
Number of reflections	22 687	7 748
Redundancy	5.8	13.2
Completeness (%)	87.1	96.0
Signal (<I/σI>)	20.7	19.2
R_{sym} (%)	10.7	12.1
Refinement and stereochemical statistics		
R_{value}	0.197‡ 0.217§	0.279# 0.292**
R_{free}	0.263‡ 0.282§	0.264# 0.278**
Average B (Å^2)		
for protein	11.48	11.48
for solvent	20.90	–
Rms deviations		
bonds (Å)	0.009	0.009
angles (°)	1.94	1.70
B values (Å^2)		
bonds/angles of main chains	0.45/0.57	0.45/0.57
bonds/angles of side chains	0.80/0.94	0.78/0.94

*Data collection statistics 30.0–2.0 Å. †Data collection statistics 30.0–3.0 Å. ‡F>2σ, 6.0–2.0 Å. §All F, 6.0–2.0 Å. #F>2σ, 8.0–3.0 Å. **All F, 8.0–3.0 Å.

these regions is involved in a crystal lattice contact in either one or both of the CD11a-I(EDTA) and CD11a-I(Mn) structures that may be in part responsible for the slight shifts in these loops [27,28]. The shift in the relative position of the α4–β3 loop in the CD11a-I(EDTA) and CD11a-I(Mn) structures is accompanied by the presence of an intramolecular hydrogen bond in CD11a-I(EDTA), between the side chains of Asp229 and Asn129, that is not present in the CD11a-I(Mn) structure. A reason for this difference is not clear. No nearby lattice interactions exist in either structure that might directly influence this region of CD11a I domain, and Asp229 and Asn129 occur on a

Figure 2

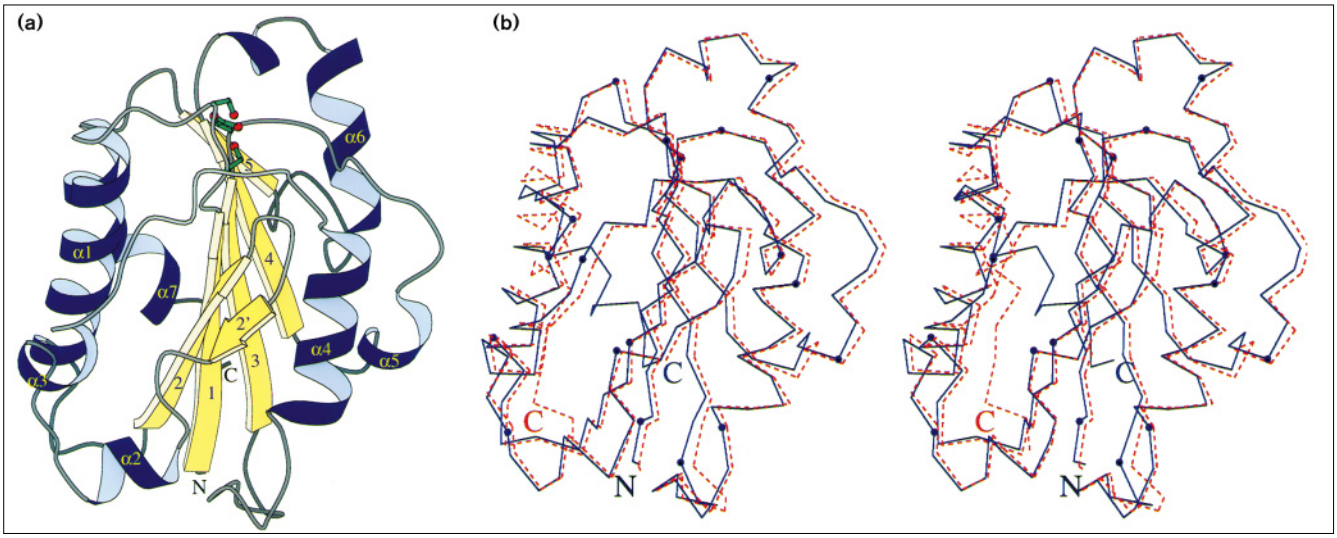

The overall fold of the CD11a I domain. (a) Ribbon diagram of CD11a-I(EDTA). The side chains of Ser139, Ser141, and Asp239 are shown in green with red oxygen atoms. The N and C termini, the β strands, and the α helical segments are labeled. (b) Stereo view of superimposed Cα backbones of CD11a-I(EDTA) (solid blue line) and CD11a-I(Mn) (dashed red line). The N and C termini are labeled and every tenth residue of CD11a-I(EDTA) is indicated by a solid circle. (Figure made with the program MOLSCRIPT [41].)

Figure 3

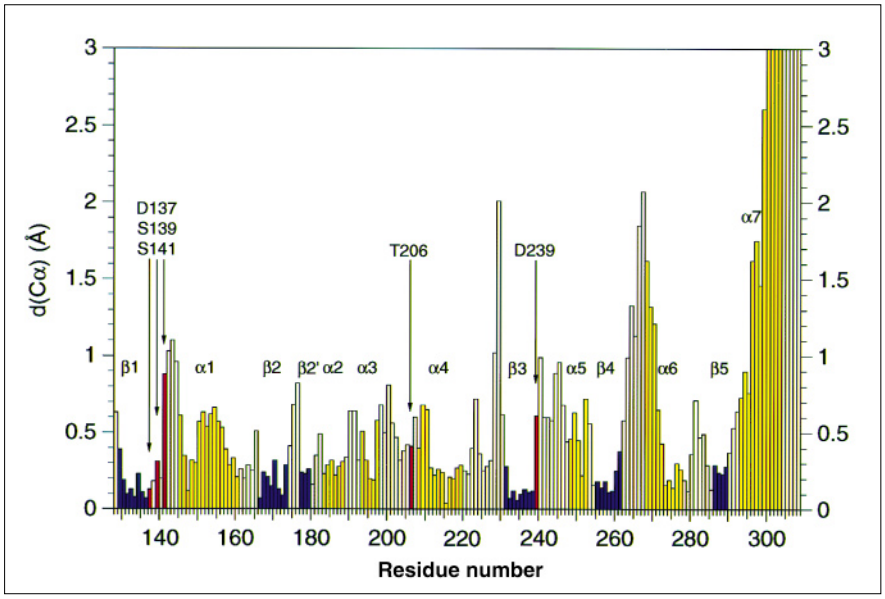

Differences in Cα positions following superposition of CD11a-I(EDTA) and CD11a-I(Mn). The higher resolution structure of the CD11a-I(Mn) determined in the C2 space group [16] was used for the comparison. Regions corresponding to the positions of β strands are colored blue, and α helical regions are colored yellow. Residues whose side chains interact directly with bound metal ion or metal-bound oxygen atoms are shown in red and labeled.

surface diametrically opposite to the CD11a I domain divalent cation binding site.

While the differences in the metal-binding site structure of CD11a-I(Mn) and CD11a-I(EDTA) are slight, the absence of the bound cation results in very different charge and surface shape in this region. Figures 4a and 4b show the molecular surfaces of CD11a-I(Mn) and CD11a-I(EDTA) colored by electrostatic charge and viewed to expose the metal-binding site. Additional differences in surface contour and charge distribution observed in these structures arise principally from the shift in the position of the α7 helix and rotameric shifts in solvent-exposed side chains. The differences observed in the vicinity of the metal-binding site result from rotameric shifts of the side chains of Lys263, His264 and Glu269. Glu241 and His264 form a salt bridge in the CD11a-I(EDTA) structure that is broken by a rotation of the His264 side chain in the CD11a-I(Mn) structure. The breaking of this salt bridge correlates with the movement of the His264-containing β4–α6 loop (see Fig. 3) and leads to greater solvent exposure of the His264 side chain. However, neither Glu241 or His264 are conserved in all I domains and the role these residues may play in ligand binding is unclear. The differing side-chain rotamers are likely due to the different lattice interactions and pH (5.2 versus 8.0) of the CD11a-I(Mn) and CD11a-I(EDTA) structures.

While the maximum distance between Cα atoms following superposition of the CD11a-I(EDTA) and CD11a-I(Mn) structures is ~2 Å for the N-terminal 166 of 181 modeled residues (see Fig. 3), distances of up to 12 Å are seen between Cα atoms in the α7 helix and C-terminal residues. Figure 5a shows the differing courses of the α7 helix in the CD11a I domain structures. As previously noted [16], an unusual packing arrangement between adjacent CD11a-I(Mn) molecules resulted in the C terminus of each molecule intercalating between the α7 helix and the body of the CD11a I domain molecule (see Fig. 5b). Examination of the regions of the CD11a I domain that contact the α7 helix in either or both of the CD11a-I(EDTA) or CD11a-I(Mn) structures, principally residues in the α1 helix and β4 and β5 strands (see Fig. 1), indicates little structural variation between these regions.

Structure of the divalent cation binding site in CD11a-I(EDTA)

Inspection of experimental and difference electron-density maps in the metal-binding site region of CD11a-I-(EDTA) revealed no density either corresponding to a strong scatterer or separated from protein atoms by distances consistent with metal coordination. Density consistent with a weak scatterer such as a sodium ion or water molecule was, however, present in the conserved divalent cation binding site (see Fig. 1a). This scatterer comes within 3 Å of six protein atoms with interatomic distances consistent with hydrogen bond lengths. The ligands surrounding this scatterer do not assume a regular geometric arrangement characteristic of metal coordination. Calculation of the valence for this site by the method of Nayal and DiCera [29] resulted in a value of 0.67. This value is inconsistent with the scattering being due to Na^+, Li^+, K^+, Mg^{2+}, or Ca^{2+}. This density has thus been modeled as a water molecule. One of the six ligands of this putative active site water molecule is the side chain of a lysine residue (Lys188) from an adjacent molecule in the crystal.

Figure 4

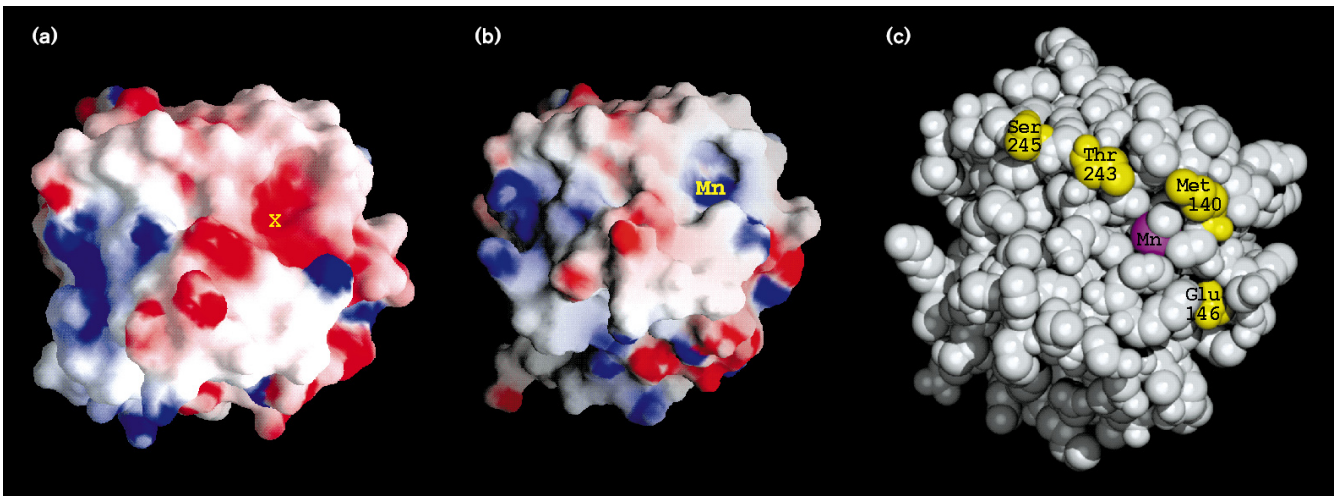

Molecular surface representations of the CD11a I domain metal-binding site: (a) CD11a-I(EDTA) and (b) CD11a-I(Mn). The molecules are displayed in similar orientations and surfaces are colored by electostatic charge with positive regions in blue and negative regions in red. The location of the manganese ion of CD11a-I(Mn) is labeled, and the location of the metal-binding site of CD11a-I(EDTA) is indicated by an 'X'. Differences in surface charge and contour occuring at the bottom of these figures result from the shift in the α7 helix. Differences occurring just below the metal-binding site result from the alternate side-chain positions assumed by Glu269 (on the left of the figure) and Lys263 and His264 (on the right of the figure). (Figures made with the program GRASP [42]). (c) Space-filling model of CD11a-I(Mn). The residue positions at which mutations affect ligand binding are colored in yellow [22]; the manganese ion is shown in magenta. (Figure made with QUANTA [Polygen, Inc.].)

A difference in metal coordination between the CD11a and CD11b I domain structures with bound manganese on the one hand and the structure of the CD11b I domain with bound magnesium, CD11b-I(Mg), on the other results in a slightly narrower metal-binding pocket in the CD11b-I(Mg) structure. This difference can be characterized by the distance between the side chain oxygen atoms of Ser141 and Thr206 and their homologues in CD11b. In the CD11a-I(Mn), CD11b-I(Mn) [15], and CD11b-I(Mg) [17] structures this serine side chain directly coordinates the metal ion, but the threonine, while directly coordinating the metal in the CD11b-I(Mg) structure, is hydrogen bonded to a metal-coordinating water in the CD11a-I(Mn) and CD11b-I(Mn) structures. The distance between the side chain oxygen atoms of these serine and threonine residues is 5.8 Å in the CD11a-I(Mn) structure while typical magnesium coordination lengths indicate that this distance must be ~4 Å in the CD11b-I(Mg) structure. This distance is 4.8 Å in the CD11a-I(EDTA) structure. Most of the difference in this distance in the CD11a-I(EDTA) and CD11a-I(Mn) structures can be attributed to a ~10° difference in both the ϕ and ψ main-chain torsion angles of Met140. These torsion angle differences result in a ~1.0 Å shift of Ser141 (and the following three residues). The main-chain hydrogen bonds observed between Ser139 and a hydrophobic loop (residues Leu203–Leu205) in CD11a-I(Mn) are thus preserved in the CD11a-I(EDTA) structure.

Discussion

We have determined the crystal structure of a metal-free form of the CD11a I domain by the MAD technique and refined this structure with diffraction data extending to 2.0 Å Bragg spacings. We have also determined the structure of a new crystal form of the CD11a I domain with bound manganese ion by molecular replacement and refined this structure with data extending to 2.0 Å Bragg spacings. The structure of the CD11a I domain with bound manganese ion was determined in this new crystal form to aid in the determination of a relatively low-resolution structure of the CD11a I domain with bound magnesium ion in an isomorphous crystal lattice. Only minor rearrangement of the metal-binding site structure is seen when the structures of the CD11a I domain with and without bound divalent cation are compared. Crystal structures of the CD11b I domain with bound magnesium ion [15] and with bound manganese ion [17] showed that the residues whose side chains interacted directly with the metal differed in these two structures. However, the residues interacting directly with the metal ion in the structures of the CD11a I domain with bound magnesium or bound manganese are the same.

Comparison of metal-free and metal-bound structures of the CD11a I domain

Evaluating the significance of conformational differences observed in the crystal structures of different forms of the same molecule is not a completely objective task. Some

Figure 5

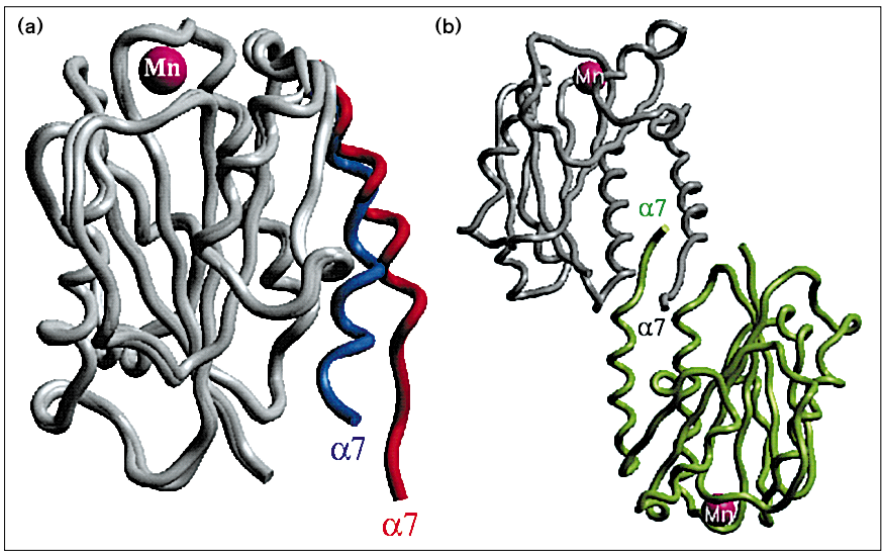

The position of the α7 helices. **(a)** Deviation of the α7 helices of CD11a-I(EDTA) and CD11a-I(Mn) following superposition. A superposition of Cα backbone traces of CD11a-I(EDTA) and CD11a-I(Mn) is shown. The α7 helix of CD11a-I(EDTA) is shown in blue, and the α7 helix of CD11a-I(Mn) is shown in red. **(b)** Dimer interaction observed in CD11a-I(Mn) and CD11a-I(Mg) crystal structures. The structures shown constitute the contents of one asymmetric unit. The α7 helices of each molecule are labeled. In both figures the manganese ions are depicted as magenta spheres. (Figures made with the program SETOR [43].)

differences can clearly result from different crystal lattice interactions, as has been shown by analysis of observed differences in multiple crystal forms of the same molecule [27,28]. Differences that result from lattice interactions are not believed to represent induced alternative conformations, but instead appear to reflect a selection of conformations from among the low-energy states normally accessible to the protein [27]. With the exception of a large movement of the α7 helix, the differences in the CD11a-I(Mn) and CD11a-I(EDTA) structures appear similar in magnitude and nature to the differences observed in different crystal forms of the same molecule. The movement observed in at least the β1–α1 loop (which contains the DXSXS divalent cation binding motif) is no doubt influenced by the presence or absence of a bound metal ion. However, this movement does not alter the secondary structure of the protein, destroy existing intraprotein interactions, create new interactions, disturb buried hydrophobic residues, or appear correlated with the larger movements of the α7 helix. Thus, we do not think that the differences observed in the metal-binding site structures of CD11a-I(Mn) and CD11a-I(EDTA) represent significantly different conformations of the CD11a I domain other than the presence or absence of a bound metal ion.

The absence of major differences in the structure of the metal-binding site of the CD11a I domain with and without bound manganese indicates that the metal is not required to stabilize a tertiary structure similar to the previously observed structures of I domains with bound manganese ion. The metal may, however, be important for stabilizing other I domain structures, such as the 'active' state observed for the CD11b I domain with bound magnesium [15,17]. The lack of notable rearrangement of the CD11a I domain in the absence of bound metal ion was not necessarily expected. We had earlier noted the presence of a strained hydrophobic loop (encompassing leucine residues 203, 204 and 205) stabilized by main-chain hydrogen bonds to the metal-coordinating loop (the DXSXS motif) and postulated that both of these loops would be likely to undergo significant rearrangement in the absence of bound cation [16]. The envisioned rearrangement clearly does not occur.

Even without large changes in the structure of the protein, the presence or absence of a bound metal ion has dramatic effects on the shape and electrostatic properties of the metal-binding site (see Fig. 4a,b). If the metal-binding site is directly involved in interactions with ligand, these altered properties could easily underlie the cation dependence of ligand binding. Several mutations that impair interactions with ligand occur at solvent-exposed positions near the metal-binding site of the CD11a I domain as shown in Figure 4c. These mutations suggest that the surface containing the metal-binding site is a contact region for the ligand ICAM-1 [22]. Curiously, mutations at the N terminus of the CD11a I domain on a surface diametrically opposite the metal-binding site disrupt interactions with ICAM-3 without affecting interactions with ICAM-1 [24].

While bound magnesium ion may be directly involved in interactions between I domains and certain ligands, the metal ion itself is unlikely to play a direct regulatory role in I domain–ligand interactions. The affinities of isolated I domains for Mg^{2+} are in the 10–100 micromolar range [6] while the extracellular concentration of Mg^{2+} is approximately millimolar and invariant. Unless the affinity of I domains for Mg^{2+} is modulated in intact integrins, the I domain metal-binding site will be constitutively occupied in physiological conditions.

While the metal-binding site of the CD11a I domain exhibits only minor changes in the presence or absence of divalent cation, the position of the α7 helix is very different in the CD11a-I(EDTA) and CD11a-I(Mn) structures. The asymmetric units of all of the structures of the CD11a I domain with bound divalent cation contain a dimer in which the C terminus of one monomer intercalates between the α7 helix and the body of the other monomer and clearly influences the disposition of the α7 helix (Fig. 5b). This interaction is not seen in the metal-free structure of the CD11a I domain, and the α7 helix in this structure is considerably less well ordered with only the general course of the helix apparent and the position of most side chains in this region indeterminate. Following superposition of metal-free and metal-bound structures of the CD11a I domain (Figs 2b,3) differences of up to 12 Å are observed between the Cα positions following the first turn of the the α7 helix.

Large changes in the position of the α7 helix are observed between structures of the CD11b I domain with either manganese or magnesium bound [17]. While similar in magnitude, these changes differ in nature from the changes observed in the CD11a I domain structures and also involve the β strand and loop preceding the α7 helix. The shift in the position of the α7 helix in the CD11a I domain structures is principally confined to regions following the first turn of the helix. The change in the position of the α7 helix in the CD11b structures appears correlated with changes in metal-binding site structure and exposure of two key hydrophobic residues, Phe275 and Phe302; it has been suggested that these changes represent a transition from low- to high-affinity forms of the CD11b I domain. The homologous phenylalanine residues of the CD11a I domain do not shift significantly and remain buried in both the metal-free and metal-bound structures. This observation indicates the α7 helix to be a labile structure in isolated I domains independent of correlated movements in the metal-binding site. The free energies of 'active' and 'inactive' forms of I domains are likely to be similar [17,30], and it will be interesting to see the I domain conformation with bound ligand if such co-crystals can be obtained.

Metal coordination

Manganese and magnesium ions show differences in both their affinity for I domains and their ability to stimulate high-affinity ligand binding. Manganese typically has a higher affinity for I domains and is able to stimulate high-affinity ligand binding in integrins independent of other stimuli [4,6]. The same or homologous amino acid side chains interact directly with the bound metal or metal-bound water molecules and form an octahedral coordination sphere in all I domain structures. However, the nature of the interactions of specific side chains differs in the structure of the CD11b-I(Mg) when compared to the CD11a-I(Mn) and CD11b-I(Mn) structures. In the structure of CD11b-I(Mg) Thr209 directly coordinates the magnesium ion while Asp242 hydrogen bonds to a metal bound water molecule. In the structures of CD11a-I(Mn) and CD11b-I(Mn) Thr209 (Thr206 in CD11a) hydrogen bonds to a metal-bound water while Asp242 (homologous to Asp239 in CD11a) directly coordinates the manganese ion. A direct interaction that occurs between a glutamic acid side chain from an adjacent molecule in the crystal lattice and the magnesium ion in the CD11b-I(Mg) structure is not present in the I domain structures with bound manganese. The presence of the same type of metal coordination in the structure of CD11a-I(Mg), as seen in the earlier I domain structures with bound manganese, indicates that the differences in coordination in the CD11b structures are not a consequence of whether magnesium or manganese is bound. As also noted by Lee *et al.* [17], it is thus likely that the differences in metal coordination are principally due to the participation of the bound magnesium in the CD11b I domain structure in a crystal lattice interaction.

While structures of isolated I domains in various contexts provide valuable insight into integrin function, many questions remain. Regions outside of the I domain have also been implicated in the interactions of I domain-containing integrins with ligands [20,31], and the role or roles played by these regions and their relationship to the I domain is poorly understood. The β chains of I domain containing integrins also contain a divalent cation binding motif, that is probably embedded in an I domain like structure, and is essential for ligand binding. The specific roles played by each metal-binding site in ligand binding need to be understood. The possibility also exists that dramatic changes in I domain tertiary structure may not underlie different affinity states. Changes in integrin quaternary structure or interactions with other molecules may also influence integrin affinity for ligand.

Biological implications

The affinity of many integrins for ligand may be increased in response to appropriate cellular stimuli by a mechanism that is believed to involve a conformational change in the integrin. High affinity interactions between members of the integrin family of receptors and their ligands are typically dependent on the presence of divalent cations. The α subunits of a subset of integrins contain an inserted or 'I' domain ~200 amino acids in length that appears to play a significant role in ligand interactions. It has been proposed that the cation dependence of integrin interactions results from either the stabilization of an active structure by the metal ion, or the direct participation of the bound metal ion in interactions with the ligand. Earlier structures of I domains from CD11a (with bound manganese) and CD11b (with bound magnesium and manganese) have identified a conserved metal-binding

site. In the case of CD11b, the structures revealed a conformational change between manganese- and magnesium-bound forms of the I domain that has been proposed to reflect high- and low-affinity states of the I domain.

We report here crystal structures of the CD11a I domain in the absence of bound metal ion and in the presence of bound magnesium ion. No large differences are observed in the structures of the metal-binding site of the CD11a I domain with and without bound manganese ion. The cation dependence of ligand binding is thus not likely to be due to stabilization of a structure similar to the I domain structures with bound manganese. Unlike the case for the CD11b I domain, no differences in the residues whose side chains directly coordinate the metal ion are observed between manganese- and magnesium-bound structures of the CD11a I domain, indicating that any differences in metal coordination are not dependent on the specific cation bound to the I domain. As in the case of the CD11b I domain structures, a significant shift in the position of an **α** helix, **α**7, is observed in different crystal forms of the CD11a I domain. These shifts are not, however, correlated with changes in the metal-binding site.

Materials and methods

Expression and purification of the CD11a I domain

The CD11a I-domain was expressed as described previously [16]. Briefly, a region of the CD11a gene encoding residues Cys125 to Gly311 was subcloned into the pET11c expression vector (Novagen) and transformed into *E. coli* strains BL21(DE3) and 834(DE3) [32]. Protein expression was induced in log phase growth cells by addition of isopropyl-β-D-thiogalactopyranoside (IPTG) and cells were harvested 3–4 h after induction. Following lysis of the cells by sonication, most of the CD11a I domain protein was found in the insoluble fraction of the lysate. This fraction was resolubilized in 7M urea, 10 mM Tris pH 7.5, 40 mM β-mercaptoethanol (β-ME), and either 5 mM $MnCl_2$, 5 mM $MgCl_2$, or 5 mM ethylenediaminetetraacetic acid (EDTA) and dialyzed in successive steps over 2 days into 10 mM Tris pH 7.5, 5 mM β-ME, and either 5 mM $MnCl_2$, 5 mM $MgCl_2$, or 2 mM EDTA. A precipitate was removed by centrifugation, and the supernatant was concentrated and loaded on to a Mono Q column (Pharmacia). In all cases the CD11a I domain protein passed through the column and was estimated to be greater than 98% pure by polyacrylamide gel electrophoresis. The CD11a I domain protein was concentrated and dialyzed into 5 mM β-ME, and either 5 mM $MnCl_2$, 5 mM $MgCl_2$, or 2 mM EDTA. Selenomethionyl-substituted protein was prepared by using the methionine-auxotrophic strain 834(DE3) as described [33] and was purified in the same manner as native protein.

Crystallization of the CD11a I domain

All crystals were grown from hanging drops by the method of vapor diffusion. Mn^{2+}-bound, Mg^{2+}-bound, and metal-free forms of CD11a I domain crystals were prepared with protein refolded and dialyzed in the presence of the appropriate cation or EDTA. Diffraction-quality crystals of metal-free SeMet CD11a I domain protein were only obtained when the crystallization trials were carried out with degassed buffers in an anaerobic chamber. Microseeding proved useful for all forms of both native and SeMet protein crystals.

Crystallization of the CD11a I domain with bound Mn^{2+}

Crystals of the CD11a I domain with bound Mn^{2+} ion were grown by mixing 1 μl of a 15 $mgml^{-1}$ solution of CD11a I domain protein in 5 mM $MnCl_2$, 5 mM β-ME with 1 μl of a reservoir solution of 14–20% PEG 3350, 100 mM $MnCl_2$, 50 mM sodium acetate, pH 5.2 and equilibrating the mixture over the reservoir solution as described previously [16]. Crystals grew to a typical size of 0.2×0.1×0.1 mm in 3–7 days. Most Mn^{2+} crystals are in space group C2 with unit cell dimensions a = 131.13 Å, b = 45.45 Å, c = 66.13 Å, and β = 99.8°, but some Mn^{2+} crystals are in space group $P2_12_12$ with unit cell dimensions a = 76.16 Å, b = 78.63 Å, and c = 66.37 Å. The asymmetric unit of both of these crystal forms contains two molecules.

Crystallization of the CD11a I domain with bound Mg^{2+}

Crystals of the CD11a I domain with bound Mg^{2+} ion were grown by mixing 1 μl of a 15 $mgml^{-1}$ solution of CD11a I domain protein in 5 mM $MgCl_2$, 5 mM β-ME with 1 μl of a reservoir solution of 14–20% PEG 3350, 100 mM $MgCl_2$, 50 mM sodium acetate, pH 5.2 and equilibrating the mixture over the reservoir solution. Crystals grew to ~0.03×0.03×0.2 mm over 3–7 days and are in space group $P2_12_12$ with unit cell dimensions a = 75.56 Å, b = 78.32 Å, and c = 66.28 Å with two molecules in the asymmetric unit.

Crystallization of metal-free CD11a I domain

Crystals of metal-free CD11a I domain were grown by mixing 1 μl of a 10–20 $mgml^{-1}$ solution of CD11a I domain protein in 2 mM EDTA, 5 mM β-ME with 1 μl of a reservoir solution of 30–33% PEG 3350, 1 mM EDTA, 30 mM Tris pH 8.0, 2 mM β-ME and equilibrating the mixture over the reservoir solution. Crystals grew to a final size of 0.04×0.03×0.2 mm over 3–7 days and are in space group $P2_12_12_1$ with unit cell dimensions a = 63.09 Å, b = 63.69 Å, and c = 40.19 Å.

Data collection and processing

All data were collected from crystals soaked for at least 15 minutes in reservoir buffer containing 10% w/v ethylene glycol and flash frozen in a gaseous nitrogen stream at –180°C. Native data from Mg^{2+}, Mn^{2+}, and metal-free crystal forms of the CD11a I domain were collected with an R-axis IIc detector and CuK^{α} radiation from a Rigaku RU200 rotating anode. MAD data from SeMet metal-free CD11a I domain crystals were collected at four wavelengths 0.9879, 0.9793, 0.9791 and 0.9686 Å (Table 2) at beamline X-4A of the National Synchrotron Light Source at Brookhaven National Laboratory using phosphor-imaging plates as detectors. Oscillations of 2.5° per image with no overlap were collected at φ and φ+180° for each wavelength.

All diffraction images were processed using the program DENZO and scaled with the program SCALEPACK [34]. <I+> and <I–> were used for MAD phase determination and partially recorded reflections were used in all cases. Diffraction data from different wavelengths were scaled with WVLSCL, and F_As and optimal f′ and f″ were calculated with MADLSQ [35].

Determination of the structure of the metal-free CD11a I domain

The structure of the metal-free form of the CD11a I domain was determined by the MAD technique with SeMet protein [36]. Four selenium sites were deduced from inspection of F_A Patterson and difference Fourier maps. Phase determinations were performed with the program MLPHARE [37], and solvent-flattening and histogram matching were performed with the program DM [38]. The initial electron-density maps calculated at 3.0 Å resolution allowed unambiguous positioning of the Mn^{2+} structure within these maps, this structure was used as a guide when building the metal-free structure. Residues from Gly128 to Phe292, corresponding to all of the I domain except the α7 helix, could be confidently placed in the initial electron-density maps. Clear helical density existed for residues beyond Phe292, but this density was relatively poorly defined and precluded precise placement of side chains. Several rounds of simulated annealing and/or Powell minimization with the program X-PLOR [39] alternated with model building with the program O [40] resulted in the current model consisting of residues Gly128 to Val308 (1458 nonhydrogen protein atoms) and 110 water

molecules. Refinement statistics and stereochemical parameters for this model are shown in Tables 1 and 3.

Determination of the structure of the Mn^{2+}-bound form of the CD11a I domain

The structure of the Mn^{2+}-bound form of the CD11a I domain in space group $P2_12_12$ was solved by molecular replacement using the structure of the Mn^{2+}-bound form of this domain solved in the space group C2 [16] as the search model. Rotation and translation functions were performed with the program X-PLOR and resulted in unambiguous solutions for two independent molecules in the asymmetric unit. Successive rounds of Powell minimization with X-PLOR alternated with model building with the program O resulted in the current model consisting of residues Gly128 to Glu310 for each molecule in the asymmetric unit (2950 total protein atoms), two manganese, two chloride ions, and 247 water molecules. Refinement statistics and stereochemical parameters for this model are shown in Table 4.

Determination of the structure of the Mg^{2+}-bound form of the CD11a I domain

The structure of the Mg^{2+}-bound form of the CD11a I domain was determined by rigid-body refinement of the structure of the Mn^{2+}-bound structure determined in the $P2_12_12$ space group. Prior to the rigid-body refinement the Mn^{2+}-bound structure was subjected to two independent simulated annealing refinements starting at 800 K. Atoms within 8 Å of the manganese ion bound to one of the I domains in the asymmetric unit were omitted from one refinement, and atoms within 8 Å of the manganese ion bound to the other I domain in the asymmetric unit were omitted from the second refinement. The results of both of these simulated annealings were used in rigid-body refinements versus the diffraction data from the Mg^{2+}-containing crystals. Electron-density maps were calculated from each refinement with $(2F_o–F_c)$ coefficients from which atoms within an 8 Å sphere around the corresponding manganese ion were omitted from the map calculation. Inspection of these maps resulted in minor adjustments to the side chains of nine amino acids, but no further refinement was undertaken. The rebuilt model was used to recalculate the omit maps and inspect the metal-coordination. Refinement statistics and stereochemical parameters are shown in Table 4.

Accession numbers

Atomic coordinates and structure factors have been deposited in the Brookhaven Protein Data Bank: CD11a I domain without bound cation PDB ID code 1ZON, and for related structure factors R1ZONSF; CD11a-I(Mg) PDB ID code 1ZOO, and for related structure factors R1ZOOSF; Cd11a-I(Mn) PDB ID code 1ZOP, and for related structure factors R1ZOPSF.

Acknowledgements

We thank T Hall, A. Libson, N Goffeney, S Leonard, C Ogata and the staff at beamline X-4A for assistance during synchrotron data collection, E DiCera and M Nayal for valence calculations, and T Hall and J Berg for critical comments on this manuscript. Beamline X-4A of the National Synchrotron Light Source at Brookhaven National Laboratory is supported by the Howard Hughes Medical Institute. This work was supported by awards to DJL from the American Cancer Society, the Searle Scholars program, the National Institutes of Health, and the Lucille P Markey Charitable Trust.

References

1. Hynes, R.O. (1992). Integrins: versatility, modulation, and signaling in cell adhesion. *Cell* **69**, 11–25.
2. Harvey, J.E., Hogg, N. & Landis, R.C. (1993). LFA-1 and the ICAMs. In *Lymphocyte Adhesion Molecules.* (Shimizu, Y., ed.), pp. 26–54, R.G. Landes Company, Austin, TX, USA.
3. Diamond, M.S. & Springer, T.A. (1994). The dynamic regulation of integrin adhesiveness. *Curr. Biol.* **4**, 506–517.
4. Smith, J.W. & Cheresh, D.A. (1991). Labeling of integrin $\alpha_V\beta_3$ with ^{58}Co(III). *J. Biol. Chem.* **266**, 11429–11432.
5. Dransfield, I., Cabanas, C., Craig, A. & Hogg, N. (1992). Divalent cation regulation of the function of the leukocyte integrin LFA-1. *J. Cell Biol.* **116**, 219–226.
6. Michishita, M., Videm, V. & Arnaout, M.A. (1993). A novel divalent cation-binding site in the A domain of the β2 integrin CR3 (CD11b/CD18) is essential for ligand binding. *Cell* **72**, 857–867.
7. Larson, R.S., Corbi, A.L., Berman, L. & Springer, T. (1989). Primary structure of the leukocyte function-associated molecule-1 α subunit: an integrin with an embedded domain defining a protein superfamily. *J. Cell Biol.* **120**, 703–712.
8. Colombatti, A. & Bonaldo, P. (1991). The superfamily of proteins with von Willebrand factor type A-like domains: one theme common to components of extracellular matrix, hemostasis, cellular adhesion, and defense mechanisms. *Blood* **77**, 2305–2325.
9. Diamond, M.S., Garcia-Aguilar, J., Bickford, J.K., Corbi, A.L. & Springer, T.A. (1993). The I-domain is a major recognition site on the leukocyte integrin Mac-1 (CD11b/CD18) for four distinct ligands. *J. Cell Biol.* **120**, 1031–1043.
10. Landis, R.C., McDowall, A., Holness, C.L.L., Littler, A.J., Simmons, D.L. & Hogg, N. (1994). Involvement of the 'I' domain of LFA-1 in selective binding to ligands ICAM-1 and ICAM-3. *J. Cell Biol.* **126**, 529–537.
11. Randi, A.M. & Hogg, N. (1994). I domain of β2 integrin lymphocyte function-associated antigen-1 contains a binding site for ligand intercellular adhesion molecule-1. *J. Biol. Chem.* **269**, 12395–12398.
12. Bilsland, C.A.G., Diamond, M.S. & Springer, T.A. (1994). The leukocyte integrin p150,95 (CD11c/CD18) as a receptor for iC3b. *J. Immunol.* **152**, 4582–4589.
13. Kamata, T. & Takada, Y. (1994). Direct binding of collagen to the I domain of integrin α2β1 (VLA-2, CD49b/CD29) in a divalent cation-dependent manner. *J. Biol. Chem.* **269**, 26006–26010.
14. Kern, A., Briesewitz, R., Bank, I. & Marcantonio, E.E. (1994). The role of the I domain in ligand binding of the human integrin α1β1. *J. Biol. Chem.* **269**, 22811–22816.
15. Lee, J., Rieu, P., Arnaout, M.A. & Liddington, R. (1995). Crystal structure of the A domain from the α subunit of integrin CR3 (CD11b/CD18). *Cell* **80**, 631–638.
16. Qu, A. & Leahy, D.J. (1995). Crystal structure of the I-domain for the CD11a/CD18 (LFA-1, $\alpha_L\beta_2$) integrin. *Proc. Natl. Acad. Sci. USA* **92**, 10277–10281.
17. Lee, J.-O., Bankston, L.A., Arnaout, M.A. & Liddington, R.C. (1995). Two conformations of the integrin A-domain (I-domain): a pathway for activation. *Structure* **3**, 1333–1340.
18. Andersen, R.D., *et al.*, & Ludwig, M.L. (1972). Structure of the radical form of clostridial flavodoxin: a new molecular model. *Proc. Natl. Acad. Sci. USA* **69**, 3189–3191.
19. Rossman, M.G., Moras, D. & Olsen, K.W. (1974). Chemical and biological evolution of a nucleotide-binding protein. *Nature* **250**, 194–199.
20. Bajt, M.L., Goodman, T. & McGuire, S.L. (1995). β2 (CD18) mutations abolish ligand recognition by I domain integrins LFA-1 ($\alpha_L\beta_2$, CD11a/CD18) and MAC-1 ($\alpha_M\beta_2$, CD11b/CD18). *J. Biol. Chem.* **270**, 94–98.
21. Edwards, C.P., *et al.*, & Bodary, S.C. (1995). Identification of amino acids in the CD11a I-domain important for binding of the leukocyte function-associated antigen-1 (LFA-1) to intercellular adhesion molecule-1 (ICAM-1). *J. Biol. Chem.* **270**, 12635–12640.
22. Huang, C. & Springer, T.A. (1995). A binding interface on the I domain of lymphocyte function-associated antigen-1 (LFA-1) required for specific interaction with intercellular adhesion molecule 1 (ICAM-1). *J. Biol. Chem.* **270**, 19008–19016.
23. D'Souza, S.E., *et al.*, & Smith, J.W. (1994). Ligand and cation binding are dual functions of a discrete segment of the integrin β_3 subunit: cation displacement is involved in ligand binding. *Cell* **79**, 659–667.
24. van Kooyk, Y., *et al.*, & Bodary, S.C. (1996). Critical amino acids in the lymphocyte function associated antigen 1 I domain mediate intercellular adhesion molecule 3 binding and immune function. *J. Exp. Med.* **183**, 1247–1252.
25. Brunger, A.T. (1992). The free R value: a novel statistical quantity for assessing the accuracy of crystal structures. *Nature* **355**, 472–474.
26. Hodel, A., Kim, S.-H. & Brunger, A.T. (1992). Model bias in macromolecular crystal structures. *Acta Cryst. A* **48**, 851–858.
27. Kossiakoff, A.A., Randal, M., Guenot, J. & Eigenbrot, C. (1992). Variability of conformations at crystal contacts in BPTI represent true low-energy structures: correspondence among lattice packing and molecular dynamics structures. *Proteins* **14**, 65–74.
28. Zhang, X.J., Wozniak, J.A. & Matthews, B.W. (1995). Protein flexibility and adaptability seen in 25 crystal forms of T4 lysozyme. *J. Mol. Biol.* **250**, 527–552.
29. Nayal, M. & Di Cera, E. (1996). Valence screening of water in protein crystals reveals potential Na^+ binding sites. *J. Mol. Biol.* **256**, 228–234.

30. Cai, T.-Q. & Wright, S.D. (1995). Energetics of leukocyte integrin activation. *J. Biol. Chem.* 270, 14358–14365.
31. Stanley, P., Bates, P.A., Harvery, J., Bennett, R.I. & Hogg, N. (1994). Integrin LFA-1 alpha subunit contains an ICAM-1 binding site in domains V and VI. *EMBO J.* 13, 1790–1798.
32. Studier, F.W., Rosenberg, A.H., Junn, J.J. & Dubendorff, J.W. (1990). Use of T7 RNA polymerase to direct expression of cloned genes. *Methods Enzymol.* 185, 60–89.
33. Leahy, D.J., Erickson, H.P., Aukhil, I., Joshi, P. & Hendrickson, W.A. (1994). Crystallization of a fragment of human fibronectin: introduction of methionine by site-directed mutagenesis to allow phasing via selenomethionine. *Proteins* 19, 48–54.
34. Otwinowski, Z. (1993). Oscillation Data Reduction Program. In *Proceeding of the CCP4 Study Weekend*: *Data Collection and Processing*. (Sawyer, L., Isaacs, N. & Bailey, S., eds), pp. 56–62 Daresbury Laboratory, Warrington, UK.
35. Hendrickson, W.A. (1991). Determination of macromolecular structures from anomalous diffraction of synchrotron radiation. *Science* 254, 51–58.
36. Hendrickson, W.A., Horton, J.R. & LeMaster, D.M. (1990). Selenomethionyl proteins produced for analysis by multiwavelength anomalous diffraction (MAD): a vehicle for direct determination of three-dimensional structure. *EMBO J.* 9, 1665–1672.
37. Collaborative Computational Project No. 4. (1994). The CCP4 suite: programs for protein crystallography. *Acta Cryst. D* 50, 760–763.
38. Zhang, K.Y.J. & Main, P. (1990). Histogram matching as a new density modification technique for phase refinement and extension of phases. *Acta Cryst. A* 46, 41–46.
39. Brunger, A.T. (1992). *X-PLOR, Version 3.1. A System for X-ray Crystallography and NMR.* Yale University Press, New Haven, CT.
40. Jones, T.A. & Kjeldgaard, M. (1991). Improved methods for the building of protein models in electron density maps and the location of errors in these models. *Acta Cryst. A* 47, 110–119.
41. Kraulis, P.J. (1991). MOLSCRIPT: a program to produce both detailed and schematic plots of proteins. *J. Appl. Cryst.* 24, 946–950.
42. Nicholls, A., Sharp, K.A. & Honig, B. (1991). Protein folding and association; insights from the interfacial and thermodynamic properties of hydrocarbons. *Proteins* 11, 281–296.
43. Evans, S.V. (1993). SETOR: hardware lighted three-dimensional solid model representations of macromolecules. *J. Mol. Graph.* 11, 134–138.